Published in final edited form as:
Biochemistry. 2010 July 13; 49(27): 5662–5670. doi:10.1021/bi100710a.

Structure and Properties of a Bis-Histidyl Ligated Globin from *Caenorhabditis elegans*[†]

Jungjoo Yoon[‡], **Mark A. Herzik Jr.**[‡,§], **Michael B. Winter**[‡,∥], **Rosalie Tran**[‡,∥], **Charles Olea Jr.**[‡,§], and **Michael A. Marletta**[*,‡,§,∥,⊥]

[‡]California Institute for Quantitative Biosciences, University of California, Berkeley, California 94720

[§]Department of Molecular and Cell Biology, University of California, Berkeley, California 94720

[∥]Department of Chemistry, University of California, Berkeley, California 94720

[⊥]Division of Physical Biosciences, Lawrence Berkeley National Laboratory, California 94720

Abstract

Globins are heme-containing proteins that are best known for their roles in oxygen (O_2) transport and storage. However, more diverse roles of globins in biology are being revealed, including gas and redox sensing. In the nematode *Caenorhabditis elegans*, 33 globin or globin-like genes have been recently identified, some of which are known to be expressed in the sensory neurons of the worm and linked to O_2 sensing behavior. Here, we describe GLB-6, a novel globin-like protein expressed in the neurons of *C. elegans*. Recombinantly expressed full-length GLB-6 contains a heme site with spectral features that are similar to those of other bis-histidyl ligated globins, such as neuroglobin and cytoglobin. In contrast to these globins, however, ligands such as CO, NO, and CN^- do not bind to the heme in GLB-6, demonstrating that the endogenous histidine ligands are likely very tightly coordinated. Additionally, GLB-6 exhibits rapid two-state autoxidation kinetics in the presence of physiological O_2 levels as well as a low redox potential (−193 ± 2 mV). A high resolution (1.40 Å) crystal structure of the ferric form of the heme-domain of GLB-6 confirms both the putative globin-fold and bis-histidyl ligation and also demonstrates key structural features that can be correlated with the unusual ligand binding and redox properties exhibited by the full-length protein. Taken together, the biochemical properties of GLB-6 suggest that this neural protein would most likely serve as a physiological sensor for O_2 in *C. elegans* via redox signaling and/or electron transfer.

Globins are hemoproteins of about 150 amino acids comprised of five to eight α-helices that adopt the classic globin fold. The heme *b*, or protophorphyrin IX, cofactor typically exists in either the reduced ferrous [Fe(II)] or oxidized ferric [Fe(III)] oxidation state. The heme iron center is coordinated equatorially by four pyrrole nitrogens from the porphyrin, and one of the two axial sites is invariably occupied by a histidine residue, often called the proximal histidine. The coordination at the remaining axial, or distal, site varies between different

[†]This study was funded by National Institutes of Health Grant GM077365 (M.A.M) and supported by the America Heart Association Western States Affiliate Postdoctoral Fellowship Program (J.Y.).

[*]Address correspondence to Michael A. Marletta, QB3 Institute, 570 Stanley Hall, University of California, Berkeley, CA 94720-3220, marletta@berkeley.edu. Tel: 510-666-2763., Fax: 510-666-2765.

SUPPORTING INFORMATION

Supporting Information Available: MALDI-TOF spectra of GLB-6. This material is available free of charge via the Internet at http://pubs.acs.org.

PDB Accession Code: 3MVC

globins. In myoglobin (Mb) or hemoglobin (Hb), this distal site remains open in the ferrous state, allowing exogenous ligands, such as O_2, CO and NO, to reversibly bind. Alternatively, the distal site in neuroglobin (Ngb) or cytoglobin (Cgb) is occupied by a second histidine, forming a bis-histidyl ligated heme site (1–4), which plays an important role in tuning heme ligand binding and redox potentials in these globin proteins (5,6).

The globins have been mainly recognized as respiratory proteins involved in O_2 storage and transport, based on our extensive knowledge of vertebrate Mb and Hb. However, genome libraries have revealed a plethora of globin and globin-like proteins varying in size, properties, and functions. Ngb and Cgb, which are found in nervous tissues (7) and non-neuronal cells (8), respectively, are two of the most recent additions to the family of vertebrate globins. The physiological function of these vertebrate globins is unclear, although a possible role for Ngb has been proposed in protecting neurons against hypoxia and ischemic injury (9–11). Non-vertebrate globins, on the other hand, are more diverse and have a wider variety of physiological functions (12,13). These globins range from single domain globins to multi-domain and multi-subunit chimeric proteins containing both globin and non-globin domains. These include bacterial flavohemoglobins, which are proposed to detoxify NO through a reaction that forms nitrate (14–17), and globin-coupled sensor proteins, such as HemAT found in the archaeon *Halobacterium salinarum* and the gram-positive bacterium *Bacillus subtilis*(18), which are involved in aerotaxis transduction (19,20).

In the nematode *Caenorhabditis elegans*, it was shown with reverse transcription polymerase chain reaction (RT-PCR) that 33 globin or globin-like genes are expressed (21–23). While little is still known about their function and biochemical properties, it has recently been shown that some of these globins may participate in a gas sensory signaling pathway in *C. elegans*. In particular, Bargmann and co-workers (24) and De Bono and co-workers (25) have independently shown that a neural globin, GLB-5, plays an important role in O_2-dependent behavioral responses in wild-type strains of *C. elegans*. These studies have demonstrated that GLB-5 functions as an O_2 sensor in the gas sensory neurons and modulates the neuronal and behavioral responses of the worm to changes in O_2 concentration (26,27). In addition, De Bono and co-workers have shown that recombinant GLB-5 exhibits absorption spectra that are very similar to those of Ngb and Cgb, indicative of a bis-histidyl ligated heme site (25). They further noted that GLB-5 oxidizes rapidly through reversible binding of O_2, which would be an important feature for a signaling protein.

In this study, we present a detailed biochemical characterization of a *C. elegans* neural globin, GLB-6. Using spectroscopic, kinetic, and potentiometric methods, we demonstrate that this protein is a heme-binding protein with ligand binding and redox properties that are unusual for globins. Furthermore, we present a crystal structure of the heme domain of GLB-6 to provide a molecular level description of its novel globin-fold structure and a correlation to its biochemical properties. Taken together, we propose that GLB-6 could function as a redox sensor in *C. elegans*, playing an important role in O_2 sensing in these worms.

MATERIALS AND METHODS

Construction of Expression Plasmids

Complementary DNA (cDNA) of the *glb-6* gene from *C. elegans* strain N2 was provided by Prof. Cornelia Bargmann (The Rockefeller University, New York), which was obtained using RT-PCR as previously described (24). The cDNA was cloned into the PET-28b expression vector (Novagen) that was modified to include an N-terminal His_6-tag followed

by a tobacco etch virus (TEV) protease recognition site (ENLYFQG). As a result, the expression sequence of GLB-6 included an N-terminal sequence, MGSSHHHHHHSSGENLYFQGH, before the starting M1 residue.

Protein Expression

The expression vectors were transformed into *E. coli* Rosetta 2(DE3) cells (Novagen). Antibiotic selection was carried out with 35 μg/mL kanamycin and 34 μg/mL chloramphenicol. For expression, *E. coli* were grown in 4 L beveled flasks, each containing 1 L of modified Terrific Broth (12 g of casein enzymatic hydrolysate, 24 g of yeast extract, 4 mL of glycerol, 17 mM KH_2PO_4, and 72 mM K_2HPO_4). Cultures were grown at 37 °C to an OD_{600} of ~0.6. Upon induction with 1 mM isopropyl β-D-1-thiogalactopyranoside, 0.5 mM 5-aminolevulinic acid was also added to facilitate heme biosynthesis. Induction was allowed to occur at 25 °C for 17 hours before cells were collected by centrifugation and stored at −80 °C.

Protein Purification

Frozen cells were thawed on ice and resuspended in lysis buffer (50 mM sodium phosphate, pH. 8.0, 150 mM NaCl, 1 mM Pefabloc (Pentapharm), 1 mM benzamidine, 5 mM β-mercaptoethanol, and 5 % glycerol) with the addition of DNaseI and lysozyme (Sigma). Resuspended cells were lysed by homogenization with an Emulsiflex-C5 high-pressure homogenizer at 20000 psi (Avestin, Inc.). Lysed cells were centrifuged at 200000 g for 1 hour. The supernatant was collected and applied to a Ni-NTA column (Qiagen) equilibrated with buffer A (50 mM sodium phosphate, pH. 8.0, 150 mM NaCl, 5 mM β-mercaptoethanol, 5% glycerol and 20 mM imidazole) at 4 °C. The column was washed with approximately ten column volumes of buffer A. GLB-6 was then eluted with buffer B (50 mM sodium phosphate, pH. 8.0, 150 mM NaCl, 5 mM β-mercaptoethanol, 5% glycerol, and 200 mM imidazole). To cleave off the N-terminal His_6-tag, TEV protease was added to the eluted protein sample at a ratio of 1:10 TEV versus GLB-6 based on A_{280}, and the solution was dialyzed overnight at 4 °C against 2 L of buffer A. The dialyzed protein solution was then passed over a freshly prepared Ni-NTA column equilibrated with buffer A. The solution was eluted with buffer A and non-tagged GLB-6 was collected as flow-through. GLB-6 was then concentrated to approximately 5 mL and loaded onto a Superdex 75 HiLoad 26/60 gel filtration column (Pharmacia) that was pre-equilibrated with buffer C (50 mM HEPES, pH. 7.5, 150 mM NaCl, 2 mM DTT and 5% glycerol) at a flow rate of 0.5 mL/min. The aliquots containing the purified protein were collected, frozen in liquid N_2, and stored at −80 °C. The yield was approximately 5 mg/L of *E. coli* culture. Purity was assessed to be > 95% by SDS-PAGE. Electrospray ion (ESI^+) mass spectrometry confirmed the expected mass (43720.1 Da versus predicted 43720.9 Da; University of California at Berkeley, QB3 Mass Spectrometry Facility).

Characterization of the GLB-6 Heme Domain

To obtain a stable heme domain construct, several C-terminal constructs (residues 187–389, 190–389, 192–389, and 196–389) were initially generated based on sequence homology with other globins. Of these constructs, only the GLB-6 (187–389) construct bound heme and expressed well (the plasmid construction, protein expression and protein purification of the heme domain constructs were performed in the same manner as the full-length GLB-6 described above).

To further define the heme domain, limited proteolysis on GLB-6 (187–389) was performed by the addition of trypsin (Trypsin Gold, Promega) to the protein sample in a 1:1000 (w:w) ratio at 37 °C. A stable fragment at ~20 kDa was seen via SDS-PAGE. Mass fingerprinting using an Applied Biosystems 4800 matrix-assisted laser desorption/ionization time-of-flight

spectrometer (MALDI-TOF, University of California at Berkeley, QB3 Mass Spectrometry Facility) was performed (Figure S1), which identified this fragment as residues M187-R355. Purified GLB-6 (187–355) was heme-bound and well expressed (protein expression and purification was performed in the same manner as the full-length GLB-6 described above) with a yield of 25–30 mg/L of *E. coli* culture. The mass was confirmed with ESI^+ mass spectrometry (20010.1 Da versus predicted 20010.9 Da).

Crystallization of the Heme-Domain of GLB-6

GLB-6 (187–355) was exchanged into 20 mM MES (pH 5.5) with 200 mM NaCl and concentrated to 60 mg/mL (3.0 mM). Crystals were grown by sitting drop vapor diffusion by mixing 1 μL of the protein solution with 1 μL of the reservoir solution (1.0 M $NaNO_3$ and 0.1 M $Na(CH_3COO)$ pH 4.5) and 1 μL of 10 mM praseodymium (III) acetate solution, which was equilibrated against 700 μL reservoir solution at 20 °C. Crystals began to appear within 6 hours. Cryoprotection was achieved by transferring the crystals stepwise into mother liquor solutions containing a final concentration of 35 % glycerol. Crystals were flash frozen and stored in liquid N_2.

X-ray Data Collection, Phasing and Refinement

X-ray data were collected by using synchrotron radiation at beamlines 5.0.3 (λ = 0.9765 Å) and 8.3.1 (λ = 1.1158 Å) at the Advanced Light Source, Lawrence Berkeley National Laboratory. Diffraction images were collected at 100 K with 1 s exposure time and 1° oscillations per frame using inverse beam geometry. Data integration and scaling were performed using the HKL2000 suite with anomalous flags selected (28). Praseodymium containing crystals (4 Pr atoms per asymmetric unit) contained sufficient anomalous signal to 2.5 Å for experimental phase determination by single-wavelength anomalous dispersion (SAD). Substructure solution, phasing, density modification and preliminary model building were carried out using *Autosol* and *Autobuild* in *PHENIX* (29). Phases were extended to 1.40 Å by using rigid-body refinement of the initial model against the highest resolution data set. Iterative model building was performed using ARP/wARP (30) and manual model building was carried out by using the program Coot (31). Refinement was carried out using *PHENIX* (29) with TLS refinement parameters incorporated. Refinement statistics are given in Table 2. Stereochemical properties were assessed by MOLPROBITY (32) and PROCHECK (33). Coordinates are deposited in the RCSB Protein Data Bank under PDB accession code 3MVC.

UV-vis Spectroscopy

Absorption spectra were recorded in an anaerobic cuvette on a Cary 3E or 300 spectrophotometer equipped with a temperature controller set at 10 °C. Spectra were recorded from proteins in a solution of buffer (20 mM HEPES pH 7.5 and 150 mM NaCl). Protein samples were prepared in an anaerobic chamber (Coy Laboratory Products) flushed with a 10:90 H_2/N_2 gas mixture (Praxair, Inc.). For both the full-length GLB-6 (1–389) and the heme-domain (187–355) construct, the ferric form was obtained upon purification. The ferrous form was prepared with the addition of sodium hydrosulfite (dithionite). Excess reductant was removed using a PD-10 desalting column (GE Healthcare) pre-equilibrated with degassed buffer in the anaerobic chamber. Ligand binding experiments with CO, NO and CN^- were performed in the following manner: For CO binding, CO (Praxair, 99.99% purity) was added to the head space of a sealed Reacti-Vial (Pierce) containing ferrous GLB-6. For NO binding, an anaerobic solution of diethylamine NONOate (Cayman) in 10 mM NaOH was added to ferrous GLB-6 in the anaerobic chamber. For CN^- binding, a solution of KCN was added directly to an aerobic solution of ferric GLB-6.

Resonance Raman Spectroscopy

Spectra were collected using 413.1 nm excitation from a Kr^+ laser (Spectra-Physics model 2025). Raman scattering was detected with a cooled, back-illuminated CCD (LN/CCD-1100/PB; Roper Scientific) controlled by an ST-133 controller coupled to a subtractive dispersive double spectrograph. The laser power at the sample was 0.3–2 mW. A microspinning sample cell was used to minimize photo-induced degradation. The typical data acquisition time was 60 min. UV-Vis absorption spectra were obtained both before and after the Raman experiments to ensure that sample integrity was maintained. The Raman spectra were corrected for wavelength dependence of the spectrometer efficiency. The instrument was calibrated using cyclohexane, carbon tetrachloride, and toluene as standard solvents. The reported frequencies are accurate to ±1 cm^{-1}, and the resolution of the spectra is 8 cm^{-1}. For each Raman spectrum, the raw data were baseline corrected, and the buffer (20 mM HEPES pH 7.5 and 150 mM NaCl) background signal was subtracted.

Stopped-Flow Spectroscopy

Autoxidation rates were determined at 10 °C on a HiTech KinetAsyst stopped-flow instrument equipped with a diode array detector. Sample preparations were carried out in an anaerobic chamber as described above. GLB-6 was reduced with ~100 molar equivalent of dithionite for >10 minutes at 4 °C. The protein was then exchanged into a buffer for spectral measurements (50 mM HEPES, pH 7.5, 150 mM NaCl) using a PD-10 desalting column. Ferrous GLB-6 was loaded into a tonometer attached to a 3-way joint that was also connected to a 30 mL Luer-Lok syringe filled with anaerobic buffer. The joints were sealed with Parafilm. Prior to data acquisition, the stopped-flow sample syringe was made anaerobic through incubation with sodium hydrosulfite (~10 mM) for >15 minutes at 10 °C. The sodium hydrosulfite was subsequently flushed from the stopped-flow syringe with ~15 mL of anaerobic buffer delivered via the 3-way joint immediately before the anaerobic, ferrous protein was loaded for analysis. Saturated O_2 solutions (1.28 mM) (34) were prepared by sparging 3–5 mL buffer in a septum-sealed vial with O_2 gas (Praxair, Inc.) for >15 minutes at room temperature. Solutions of 74.2% O_2 (950 μM) and 40.3% (516 μM) O_2 were prepared by mixing saturated O_2 solutions, delivered via a gas-tight syringe, with anaerobic buffer in a septum-sealed vial. Solutions of 21% (268 μM) O_2 were prepared with air-saturated buffer. Solutions of 10.5% (134 μM) O_2 were prepared by mixing air-saturated buffer, delivered via a gas-tight syringe, with anaerobic buffer in a septum-sealed vial. O_2 stocks were made in duplicate or triplicate. Autoxidation reactions were initiated by equal mixing on the stopped-flow with the oxygenated buffer solutions. UV-visible spectra were acquired for 4.5 to 22.5 s (300 scans, 1.5 ms integration time) from 300–700 nm using the Kinetic Studio (TgK Scientific) software package. For each independently prepared O_2 stock, 3–6 data sets were acquired. The spectral transition from 425 nm to 411 nm was fit to a two-state model using the SPECFIT Global Analysis System (Version 3.0.14).

Spectrochemical Redox Titration

Potentiometric titrations were performed as previously described (35) using an Oakton pH 1100 Series potentiometer. Titrations were carried out at 25 °C with stirring in the presence of redox mediator mix solution containing methyl viologen (−440 mV), anthraquinone-2,6-disulfonic acid (−184 mV), 2-hydroxy-1,4-naphthoquinone (−137 mV), 2,5-dihydroxy-1,4-benzoquinone (−60 mV), tetramethyl-p-benzochinon (Duroquinone) (+5 mV), 1,2-naphthoquinone (+157 mV) and ferricyanide (+356 mV). O_2 was removed from the cuvette by flushing continuously with argon. Reductive titrations were performed by stepwise addition of dithionite solution and oxidative titrations were performed by stepwise addition of ferricyanide solution. The change in the heme oxidation state was monitored by the absorbance change in the α-band at 560 nm.

RESULTS AND DISCUSSION

Spectroscopic Characterization of GLB-6

In order to characterize the spectral properties of GLB-6, the ferrous and ferric forms of the full-length protein were first investigated with UV-vis absorption spectroscopy (Figure 1). The spectrum of ferric GLB-6 exhibits a Soret band centered at 411 nm and a β band at 532 nm (dotted line, Figure 1). Ferrous GLB-6 exhibits a Soret band at 425 nm and α/β bands at 560 and 530 nm, with an α/β intensity ratio of approximately 2:1. These spectral features resemble those of cytochrome b_5 (36) and globins such as neuroglobin (5,7), cytoglobin (6) and nonsymbiotic plant hemoglobins (37,38), suggestive of a low-spin (S = 1/2 for ferric and S = 0 for ferrous heme) bis-histidyl ligated heme site (39,40). The heme domain construct of residues 187–355 also exhibits the same Soret and α/β band features as full-length GLB-6 in both the ferric and ferrous forms, indicating that the heme structures are very similar between the heme domain and the full-length constructs.

Resonance Raman spectra of the ferrous and ferric forms of GLB-6 are shown in Figure 2. The heme skeletal bands related to oxidation, coordination and spin states are found in the high frequency region. The most intense peak in this region, occurring between 1350–1370 cm^{-1}, corresponds to the C_α-N stretching mode (ν_4) and is sensitive to the oxidation state of the heme. In addition, ν_3 is the coordination- and spin state-sensitive C_α-C_m stretching mode, and is typically detected in the 1470–1500 cm^{-1} range (39,41). For GLB-6, ν_4 and ν_3 for the ferrous form are observed at 1362 cm^{-1} and 1494 cm^{-1}, respectively (Figure 2c), while those of the ferric form are observed at 1375 cm^{-1} and 1507 cm^{-1}, respectively (Figure 2d), consistent with a low-spin, bis-histidyl heme ligation in both the ferrous and ferric states. Due to the bis-histidyl state of ferrous GLB-6, no Fe-His stretching was observed in the low frequency region (at ~220 cm^{-1}) (42,43) (Figure 2a).

Ligand Binding in GLB-6

Ligand binding experiments with CO, NO, and CN^-, which are known to form highly stable complexes with ferrous (CO and NO) and ferric (CN^-) heme sites, were performed to further investigate the biochemical properties of the protein (44). Interestingly, however, it was found that GLB-6 does not bind any of these ligands. No spectral change was observed when ferrous GLB-6 was treated with NO or when ferric GLB-6 was treated with CN^-. For CO binding, a small blue-shift (~1 nm) of the Soret band (no change in the α and β band positions) and a slight decrease in the intensities of the Soret, α and β bands were observed when excess CO was added to ferrous GLB-6 anaerobically. These spectral changes are possibly due to some Fe-CO complex formation in the presence of excess CO. However, no sign of a Fe-CO or C–O stretch was observed in the resonance Raman spectrum, indicating that a very low amount of Fe-CO complex, if any, was present. Alternatively, exposing the ferrous-CO sample to air (in the presence of dithionite to prevent oxidation) resulted in regeneration of the fully reduced ferrous spectrum, likely due to the CO ligand being readily replaced by the endogenous histidine. Note that an O_2 binding experiment could not be performed due to the rapid oxidation of GLB-6. However, the fact that the affinities of CO and NO to heme centers are typically much higher than O_2 in other heme proteins (45) suggests that a stable O_2 complex with the heme iron in GLB-6 is very unlikely.

The role of bis-histidyl ligation in slowing the on-rate of exogenous ligands has been previously demonstrated in Ngb using stopped-flow and flash photolysis experiments, in which the dissociation of the distal histidine ($k_{off} \sim 1$ sec^{-1}) was shown to be the rate limiting step in CO and O_2 binding (5,46,47). However, with high intrinsic affinities for CO and O_2 for the pentacoordinate heme, Ngb is able to form stable CO and O_2 complexes. In GLB-6, the lack of ligand binding suggests that the Fe-His bonds in the GLB-6 heme site

may be stronger than those of Ngb but also that the intrinsic affinities for exogenous ligands could be low even in the absence of the distal histidine, possibly due to a heme pocket that is unfavorable for stable heme-ligand complex formation.2

Autoxidation Rate of GLB-6

During the spectral characterization of GLB-6, it was found that the ferrous protein immediately oxidized to the ferric oxidation state when exposed to air. To quantify this rapid autoxidation of GLB-6, stopped-flow experiments were performed. A spectral transition from 425 nm to 411 nm was observed upon reaction of the ferrous form of full-length GLB-6 (1–389) with varying O_2 concentrations (5.25, 10.5, 21.0, 37.1, and 50.0 % O_2, which correspond to 67, 134, 268, 475, and 640 μM O_2). In Figure 3a, spectral changes at 5.25 % O_2 are shown as representative data with the trace of A_{425} given in the inset. Note that 5.25 % O_2 is within the O_2 concentration range preferred by *C. elegans* in the wild (5–12%) (26). The reactions at all O_2 concentrations did not show any indication of the formation of an intermediate (isosbestic point at 418 nm, Figure 3A), such as a ferrous-oxy or ferric-superoxide complex. Therefore, the autoxidation rate was determined with a two-state, single-exponential model (i.e. ferrous → ferric), using a global fit analysis of the spectral window (375–700 nm). The observed first-order autoxidation rate constant k_{obs} of full-length GLB-6 as a function of O_2 concentration is shown in Figure 3b. No saturation of k_{obs} was observed even at high O_2 concentrations, and the data points were fit to a linear function with $k_{obs} = (3.72 \times 10^3\ M^{-1}\ s^{-1})[O_2] + 0.0747\ s^{-1}$ ($R^2 = 0.990$).3 Notably, the autoxidation rate of GLB-6 at ambient O_2 levels ($k_{obs} = 1.23\ s^{-1}$ at 21% O_2) is orders of magnitude faster than other bis-histidyl ligated globins (Table 1). In these proteins, electron transfer occurs between the ferrous heme to the O_2 ligand that is directly coordinated to the Fe center. Thus, autoxidation would require at least five sequential steps: (1) dissociation of the distal histidine from the heme, (2) coordination of O_2 to the heme Fe(II), (3) electron transfer from the heme Fe(II) to O_2 to generate a Fe(III)-superoxide complex, (4) dissociation of superoxide, leaving unligated Fe(III) heme, and (5) re-coordination of the distal histidine to the heme to reform a bis-histidyl Fe(III) heme site). GLB-6, on the other hand, lacks ligand binding as demonstrated above, and no intermediate was observed in the stopped-flow experiments at any O_2 concentration. Thus, the autoxidation most likely occurs via direct outer-sphere electron transfer from the ferrous heme to the unbound O_2 molecule (i.e. without direct coordination of O_2 to the heme Fe center), generating ferric heme and superoxide in one chemical step.

Redox Potential of GLB-6

To better understand the thermodynamic properties of GLB-6, the redox potential of the full-length protein was measured by potentiometric redox titration (Figure 4). A_{560} of ferrous GLB-6 (i.e. the α-band maximum) minus A_{560} of ferric GLB-6 was normalized and plotted against ambient potential (Figure 4, inset) and the data were analyzed for the best fit to the Nernst equation with n = 1 (dotted lines in Figure 4, inset). The reduction midpoint potential ($E^{0'}$) was −193 ± 2 mV versus the standard hydrogen electrode (SHE), which is comparable to those of other 6-coordinate *b*-type heme proteins (Table 2). This value is also lower than that of the $O_2/O_2^{\bullet-}$ redox couple (−160 mV) (48), demonstrating that electron transfer from the ferrous heme in GLB-6 to O_2 is a thermodynamically favorable process. Note that bis-histidyl ligated proteins generally exhibit lower redox potentials than those with different axial ligands, such as cytochromes c/c_{551}, cellobiose dehydrogenase with Met/

[2]All attempts to express and purify distal and proximal histidine mutants were not successful. The histidine mutants either did not express well (H254G and H286G) or did not contain heme (H254L/V/Q/M and H286M).

[3]The non-zero y-intercept (0.075 s^{-1}) in the O_2 titration reflects the small experimental error in the GLB-6 autoxidation rate. This error represents only 6% of the rate measured at ambient O_2 levels (1.23 s^{-1}).

His (49–51) and Mb with H_2O/His (52) (Table 2). Importantly, mutants with bis-histidyl ligation exhibit redox potentials that are ~200 mV lower than those of the corresponding wild type proteins. Thus, bis-histidyl ligation is a major factor in keeping the potential relatively low in GLB-6, which would be particularly critical if the protein is physiologically involved in electron transfer.

Crystal Structure of the Heme Domain of GLB-6

To gain structural insight into the biochemical properties of GLB-6, a high resolution crystal structure of the heme domain (residues 187–355) in the ferric form was solved to 1.40 Å by SAD analysis. The structure was refined to a final R_{work} of 16.1 % (R_{Free} of 20.1 %) (Table 3). The refined structure of ferric GLB-6 was built in a primitive monoclinic ($P2_1$) space group with two molecules in the asymmetric unit, each containing a *b*-type heme site. The final model was comprised of 156 and 153 amino acids in molecules A and B, respectively (no electron density was observed for residues 187–194 and 318–321 in molecule A and 187–194, 270–272 and 319–322 in molecule B), and it contained 139 water molecules and 4 praseodymium atoms. As shown in Figure 5, the tertiary structure of the GLB-6 heme domain consists of seven helices that correspond to the A, B, C, E, F, G and H helices, as anticipated of a globin-like domain.

The most conspicuous feature in the GLB-6 (187–355) structure is the bis-histidyl ligated heme site, which is consistent with our spectroscopic characterization (see above). The ferric iron center is ligated by H254 and H286 with Fe-N bond distances as 2.05 Å and 1.98 Å, respectively, reflecting strong Fe-N bonds. The bis-histidyl ligated heme structure is similar to those found in the crystal structures of human and murine Ngb (5,7), human Cgb (6), nonsymbiotic rice Hb (37,38) and most recently, a bacterial globin-coupled sensor from *Geobacter sulfurreducens* (53).

The GLB-6 heme domain structure exhibits several features that are distinct from those of other bis-histidyl ligated globins and help explain the unusual biochemical properties of the protein described above. Figure 6a and 6b (top) show a structural comparison between GLB-6 (red) and murine Ngb (yellow; PDB: 1Q1F), which is a good structural representative of other bis-histidyl ligated globins. The GLB-6 and Ngb structures superimpose to a relatively high degree overall (root mean square deviation over all C_α atoms = 2.211 Å). However, marked differences are found near the heme pocket where GLB-6 has an elongated E-helix and is missing a D-helix. The E-helix in GLB-6 has an extra helix loop (~4 amino acids) at the N-terminal side, and as a consequence, the distal His254 is positioned at the E11 position instead of E7 as in other globins (note that His254 is designated ‘distal’ based on sequence alignment with other globins). In addition, the D-helix is completely absent from the GLB-6 structure, and as a result, the C- and E-helices are directly connected. Importantly, these structural features could impose a tight restriction in the helical movement of the GLB-6 heme domain, partially inhibiting exogenous ligand binding.

Additionally, the F-helix in the GLB-6 structure is shorter than that of Ngb and is followed by a long F–G loop. Consequently, the proximal His286 is positioned at the end of the helix and is more exposed to the hydrophilic environment compared to Ngb in which the heme is imbedded in the hydrophobic pocket. Exposure to a more polar aqueous environment would thermodynamically favor the ferric state over the ferrous state of the heme site (54), consistent with the fact that GLB-6 exhibits a relatively low redox potential (GLB-6 = −193 mV vs. Ngb = −115 mV, Table 1) and undergoes spontaneous oxidation.

Figure 6a and 6b (bottom) show a structural comparison between GLB-6 (red) and a *G. sulfurreducens* globin-coupled sensor (blue; GsGCS, PDB: 2W31). GsGCS is a recently

reported bis-histidyl ligated globin with an elongated E-helix (with an E11 distal histidine) and a missing D-helix, similar to GLB-6. Unlike GLB-6, however, GsGCS has been shown to bind various exogenous ligands (53). The difference in the ligand binding properties of the two globins may be explained by the low structural similarity at the A-, B-, and C-helix regions. This may be due to the presence of an extra helix (the Z-helix) in GsGCS at the N-terminus, which affects the A-, B- and C-helix orientations in the tertiary structure of GsGCS. Such structural differences could result in different movement and flexibility in the two protein structures, which would undoubtedly alter ligand binding properties.

Potential Role of GLB-6

The present study indicates that GLB-6 would most likely function as a redox sensor or electron transfer protein rather than a gas transporter or storage protein as with most other globins. This is supported by the fact that exogenous ligands have no detectable affinity for the heme and that GLB-6 has rapid redox kinetics (note that only oxidation kinetics were measured in this study; however, reduction of ferric GLB-6 with dithionite also occurred instantaneously, indicating rapid reduction kinetics as well). The low affinity for exogenous ligands would be critical in maintaining a constant redox potential physiologically, which could be severely altered upon ligand binding to the heme site.

The fact that the redox potential of GLB-6 is lower than that of $O_2/O_2^{\bullet -}$ redox couple suggests that GLB-6 may directly interact with O_2 to generate superoxide, a reactive oxygen species which has been shown to play an important role in physiological responses such as transcriptional regulation, protein activation, bioenergy output, cell proliferation, and apoptosis (55,56). GLB-6 is implicated in O_2 dependent behavior in *C. elegans*, in which the overexpression of GLB-6 suppresses worm aggregation (personal communication, P. McGrath and C. Bargmann). GLB-6 is expressed in the RMG hub interneuron (57) where the aggregation and related behaviors are controlled. Thus, it is possible that GLB-6 could serve as a redox sensor that responds to oxidative stress, either directly or indirectly by the change in O_2 concentration. With rapid oxidation kinetics, GLB-6 would be ideal as a redox sensing protein.

Notably, other *C. elegans* globins have been suggested to serve as sensory proteins. As mentioned in the introduction, GLB-5 has been shown to be a bis-histidyl ligated globin protein involved in O_2 sensing (25). Most recently, another bis-histidyl ligated globin, GLB-26, has been characterized (along with GLB-1, a penta-coordinated globin that reversibly binds O_2). GLB-26 was shown to have very low affinity for exogenous ligands, suggestive of a role in O_2 reduction and redox reactions, as seen with GLB-6 (23). However, GLB-26 is reported to be expressed exclusively in the head mesodermal and stomato-intestinal muscle cells (23), in contrast to GLB-6, which is expressed in neurons. Thus, it appears that *C. elegans* has evolved to utilize globins for various sensory functions in different cells and tissues, which also explains the unusually high number of globin genes present in these worms.

Finally, although it was not the focus of present study, the non-heme domain of GLB-6 (residues 1–186) may also play a role in facilitating signal transduction. This domain currently, however, has no known function. Studies are underway to gain a better understanding of the non-heme domain of GLB-6, the possible cooperativity between the non-heme and heme domains, and the physiological role of the protein in O_2 sensing in *C. elegans*.

Supplementary Material

Refer to Web version on PubMed Central for supplementary material.

ABBREVIATIONS

Mb	myoglobin
Hb	hemoglobin
Ngb	neuroglobin
Cgb	cytoglobin
GsGCS	globin-coupled sensor

Acknowledgments

We thank Professor Cornelia Bargmann and Dr. Patrick McGrath of the Rockefeller University for providing us with the cDNA of GLB-6 and sharing valuable information concerning the physiological function of GLB-6. We thank P. Adams, J. Kuriyan, and beamline scientists at ALS 8.3.1 and 5.0.3 for helpful discussions during data collection and structure determination. We also thank the Marletta lab for critical reading of the manuscript.

REFERENCES

1. de Sanctis D, Dewilde S, Pesce A, Moens L, Ascenzi P, Hankeln T, Burmester T, Bolognesi M. Crystal Structure of cytoglobin: the fourth globin type discovered in man displays heme hexa-coordination. J Mol Biol. 2004; 336:917–927. [PubMed: 15095869]
2. Pesce A, Dewilde S, Nardini M, Moens L, Ascenzi P, Hankeln T, Burmester T, Bolognesi M. Human brain neuroglobin structure reveals a distinct mode of controlling oxygen affinity. Structure. 2003; 11:1087–1096. [PubMed: 12962627]
3. Vallone B, Nienhaus K, Matthes A, Brunori M, Nienhaus GU. The structure of carbonmonoxy neuroglobin reveals a heme-sliding mechanism for control of ligand affinity. Proc Natl Acad Sci USA. 2004; 101:17351–17356. [PubMed: 15548613]
4. Vallone B, Nienhaus K, Brunori M, Nienhaus GU. The structure of murine neuroglobin: Novel pathways for ligand migration and binding. Proteins. 2004; 56:85–92. [PubMed: 15162488]
5. Dewilde S, Kiger L, Burmester T, Hankeln T, Baudein-Crueza V, Aerts T, Marden MC, Caubergs R, Moens L. Biochemical characterization and ligand binding properties of neuroglobin, a novel member of the globin family. J Biol Chem. 2001; 276:38949–38955. [PubMed: 11473128]
6. Sawai H, Kawada N, Yoshizato K, Nakajima H, Aono S, Shiro Y. Characterization of the heme environmental structure of cytoglobin, a fourth globin in humans. Biochemistry. 2003; 42:5133–5142. [PubMed: 12718557]
7. Burmester T, Weich B, Reinhardt S, Hankeln T. A vertebrate globin expressed in the brain. Nature. 2000; 407:520–523. [PubMed: 11029004]
8. Burmester T, Ebner B, Weich B, Hankeln T. Cytoglobin: a novel globin type ubiquitously expressed in vertebrate tissues. Mol Biol Evol. 2002; 19:416–421. [PubMed: 11919282]
9. Khan AA, Wang Y, Sun Y, Mao XO, Miles E, Graboski J, Chen S, Ellerby LM, Jin K, Greenberg DA. Neuroglobin-overexpressing transgenic mice are resistant to cerebral and myocardial ischemia. Proc Natl Acad Sci USA. 2006; 103:17944–17948. [PubMed: 17098866]
10. Sun Y, Jin K, Mao XO, Zhu Y, Greenberg DA. Neuroglobin is up-regulated by and protects neurons from hypoxic-ischemic injury. Proc Natl Acad Sci USA. 2001; 98:15306–15311. [PubMed: 11742077]
11. Sun Y, Jin K, Peel A, Mao XO, Xie L, Greenberg DA. Neuroglobin protects the brain from experimental stroke *in vivo*. Proc Natl Acad Sci USA. 2003; 100:3497–3500. [PubMed: 12621155]
12. Weber RE, Vinogradov SN. Nonvertebrate hemoglobins: functions and molecular adaptations. Physiol Rev. 2001; 81:569–628. [PubMed: 11274340]
13. Vinogradov S, Moens L. Diversity of globin function: enzymatic, transport, storage, and sensing. J Biol Chem. 2008; 283:8773–8777. [PubMed: 18211906]

14. Mowat CG, Gazur B, Campbell LP, Chapman SK. Flavin-containing heme enzymes. Arch Biochem Biophys. 2010; 493:37–52. [PubMed: 19850002]
15. Nunoshiba T, Derojas-Walker T, Tannenbaum SR, Demple B. Roles of nitric oxide in inducible resistance of *Escherichia coli* to activated murine macrophages. Infect Immun. 1995; 63:794–798. [PubMed: 7532626]
16. Membrillo-Hernandez J, Coopamah MD, Anjum MF, Stevanin TM, Kelly A, Hughes MN, Poole RK. The flavohemoglobin of *Escherichia coli* confers resistance to a nitrosating agent, a "Nitric oxide Releaser," and paraquat and is essential for transcriptional responses to oxidative stress. J Biol Chem. 1999; 274:748–754. [PubMed: 9873011]
17. Gardner PR, Gardner AM, Martin LA, Salzman AL. Nitric oxide dioxygenase: an enzymic function for flavohemoglobin. Proc Natl Acad Sci U S A. 1998; 95:10378–10383. [PubMed: 9724711]
18. Zhang W, Phillips GN Jr. Structure of the oxygen sensor in *Bacillus subtilis*: signal transduction of chemotaxis by control of symmetry. Structure. 2003; 11:1097–1110. [PubMed: 12962628]
19. Hou S, Larsen RW, Boudko D, Riley CW, Karatan E, Zimmer M, Ordal GW, Alam M. Myoglobin-like aerotaxis transducers in Archaea and Bacteria. Nature. 2000; 403:540–544. [PubMed: 10676961]
20. Hou S, Freitas T, Larsen RW, Piatibratov M, Sivozhelezov V, Yamamoto A, Meleshkevitch EA, Zimmer M, Ordal GW, Alam M. Globin-coupled sensors: a class of heme-containing sensors in Archaea and Bacteria. Proc Natl Acad Sci USA. 2001; 98:9353–9358. [PubMed: 11481493]
21. Hoogewijs D, Geuens E, Dewilde S, Moens L, Vierstraete A, Vinogradov S, Vanfleteren JR. Genome-wide analysis of the globin gene family of *C. elegans*. IUBMB Life. 2004; 56:697–702. [PubMed: 15804834]
22. Hoogewijs D, Geuens E, Dewilde S, Vierstraete A, Moens L, Vinogradov S, Vanfleteren JR. Wide diversity in structure and expression profiles among members of the *Caenorhabditis elegans* globin protein family. BMC Genomics. 2007; 8:356. [PubMed: 17916248]
23. Geuens E, Hoogewijs D, Nardini M, Vinck E, Pesce A, Kiger L, Fago A, Tilleman L, De Henau S, Marden MC, Weber RE, Van Doorslaer S, Vanfleteren J, Moens L, Bolognesi M, Dewilde S. Globin-like proteins in *Caenorhabditis elegans in vivo* localization, ligand binding and structural properties. BMC Biochem. 2010; 11:17. [PubMed: 20361867]
24. McGrath PT, Rockman MV, Zimmer M, Jang H, Macosko EZ, Kruglyak L, Bargmann CI. Quantitative mapping of a digenic behavioral trait implicates globin variation in *C. elegans* sensory behaviors. Neuron. 2009; 61:692–699. [PubMed: 19285466]
25. Persson A, Gross E, Laurent P, Busch KE, Bretes H, De Bono M. Natural variation in a neural globin tunes oxygen sensing in wild *Caenorhabditis elegans*. Nature. 2009; 458:1030–1033. [PubMed: 19262507]
26. Gray JM, Karow DS, Lu H, Chang AJ, Chang JS, Ellis RE, Marletta MA, Bargmann CI. Oxygen sensation and social feeding mediated by a *C. elegans* guanylate cyclase homologue. Nature. 2004; 430:317–322. [PubMed: 15220933]
27. Chang AJ, Chronis N, Karow DS, Marletta MA, Bargmann CI. A distributed chemosensory circuit for oxygen preference in *C. elegans*. PLoS Biol. 2006; 4:e274. [PubMed: 16903785]
28. Otwinowski A, Minor W. Processing of X-ray diffraction data collected in oscillation mode. Methods Enzymol. 1997; 276:307–326.
29. Adams PD, Grosse-Kunstleve RW, Hung LW, Ioerger TR, McCoy AJ, Moriarty NW, Read RJ, Sacchettini JC, Sauter NK, Terwilliger TC. PHENIX: building new software for automated crystallographic structure determination, *Acta Crystallogr*. Sect. D. 2002; 58:1948–1954.
30. Lamzin, VS.; Perrakis, A.; Wilson, KS. The ARP/WARP suite for automated construction and refinement of protein models. In: Rossmann, MG.; Arnold, E., editors. International Tables for Crystallography. Dordrecht: Kluwer Academic Publishers; 2001. p. 720-722.
31. Emsley P, Cowtan K. Coot: model-building tools for molecular graphics, *Acta Crystallogr*. Sect. D. 2004; 60:2126–2132.
32. Davis IW, Leaver-Fay A, Chen VB, Block JN, Kapral GJ, Wang X, Murray LW, Arendall WB III, Snoeyink J, Richardson JS, Richardson DC. MolProbity: all-atom contacts and structure validation for proteins and nucleic acids. Nucleic Acids Res. 2007; 35:W375–W383. [PubMed: 17452350]

33. Laskowski RA, MacArthur MW, Moss DS, Thornton JM. PROCHECK: a program to check the stereochemical quality of protein structures. J Appl Crystallogr. 1993; 26:283–291.
34. Boon EM, Huang SH, Marletta MA. A molecular basis for NO selectivity in soluble guanylate cyclase. Nature Chem Biol. 2005; 1:53–59. [PubMed: 16407994]
35. Dutton PL. Redox potentiometry: determination of midpoint potentials of oxidation-reduction components of biological electron-transfer systems. Methods Enzymol. 1978; 54:411–435. [PubMed: 732578]
36. Ozols J, Strittmatter P. The interaction of porphyrins and metalloporphyrins with apocytochrome b5. J Biol Chem. 1964; 239:1018–1023. [PubMed: 14167616]
37. Duff SMG, Wittenberg BA, Hill RD. Expression, purification, and properties of recombinant barley (*Hordeum sp*.) hemoglobin. Optical spectra and reactions with gaseous ligands. J Biol Chem. 1997; 272:16746–16752. [PubMed: 9201978]
38. Arredondo-Peter R, Hargrove MS, Sarath G, Moran JF, Lohrman J, Olson JS, Klucas RV. Rice hemoglobins. Gene cloning, analysis, and O_2-binding kinetics of a recombinant protein synthesized in *Escherichia coli*. Plant Physiol. 1997; 115:1259–1266. [PubMed: 9390447]
39. Babcock GT, Widger WR, Cramer WA, Oertling WA, Metz JG. Axial ligands of chloroplast cytochrome b-559: Identification and requirement for a heme-cross-linked polypeptide structure. Biochemistry. 1985; 24:3638–3645. [PubMed: 2994713]
40. Choi CYH, Cerda JF, Chu H-A, Babcock GT, Marletta MA. Spectroscopioc characterization of the heme-binding sites in *Plasmodium falciparum* histidine-rich protein 2. Biochemistry. 1999; 38:16916–16924. [PubMed: 10606526]
41. Hu S, Smith KM, Spiro TG. Assignment of protoheme resonance Raman spectrum by heme labeling in myoglobin. J Am Chem Soc. 1996; 118:12638–12646.
42. Kitagawa, T. The heme protein structure and the iron-histidine stretching mode. In: Spiro, TG., editor. Biological Applications of Raman Spectroscopy: Resonance Raman Spectra of Heme and Metalloproteins. New York: John Wiley & Sons; 1988. p. 97-131.
43. Tran R, Boon EM, Marletta MA, Mathies RA. Resonance Raman Spectra of an O_2-Binding H-NOX Domain Reveal Heme Relaxation upon Mutation. Biochemistry. 2009; 48:8568–8577. [PubMed: 19653642]
44. Antonini, E.; Brunori, M. Hemoglobin and myoglobin in their reactions with ligands. Amsterdam: North-Holland Pub. Co; 1971.
45. Olson JS, Phillips J, GN. Myoglobin discriminates between O_2, NO, and CO by electrostatic interactions with the bound ligand. J Biol Inorg Chem. 1997; 2:544–552.
46. Uzan J, Dewilde S, Burmester T, Hankeln T, Moens L, Hamdane D, Marden MC, Kiger L. Neuroglobin and other hexacoordinated hemoglobins show a weak temperature dependence of oxygen binding. Biophys J. 2004; 87:1196–1204. [PubMed: 15298922]
47. Kiger L, Uzan J, Dewilde S, Burmester T, Hankeln T, Moens L, Hamdane D, Baudin-Crueza V, Marden MC. Neuroglobin ligand binding kinetics. IUBMB Life. 2004; 56:709–719. [PubMed: 15804836]
48. Sawyer DT, Valentine JS. How super is superoxide? Acc Chem Res. 1981; 14:393–400.
49. Rotsaert FAJ, Hallberg BM, de Vries S, Moenne-Loccoz P, Divne C, Renganathan V, Gold MH. Biophysical and structural analysis of a novel heme B iron ligation in the flavocytochrome cellobiose dehydrogenase. J Biol Chem. 2003; 278:33224–33231. [PubMed: 12796496]
50. Miller GT, Zhang B, Hardman JK, Timkovich R. Converting a c-type to a b-type cytochrome: Met61 to His61 mutant of *Pseudomonas* cytochrome c-551. Biochemistry. 2000; 39:9010–9017. [PubMed: 10913314]
51. Raphael AL, Gray HB. Axial ligand replaement in horse heart cytochrome c by semisynthesis. Proteins. 1989; 6:338–340. [PubMed: 2560194]
52. Dou Y, Admiraal J, Ikeda-Saito M, Krzywda S, Wilkinson AJ, Li T, Olson JS, Prince RC, Pickering IJ, George GN. Alteration of axial coordination by protein engineering in myoglobin. Bisimidazole ligation in the His64-->Val/Val68-->His double mutant. J Biol Chem. 1995; 270:15993–16001. [PubMed: 7608158]
53. Pesce A, Thijs L, Nardini M, Desmet F, Sisinni L, Gourlay L, Bolli A, Coletta M, Van Doorslaer S, Wan X, Alam M, Ascenzi P, Moens L, Bolognesi M, Dewilde S. HisE11 and HisF8 provide

bis-histidyl heme hexa-coordination in the globin domain of *Geobacter sulfurreducens* globin-coupled sensor. J Mol Biol. 2009; 386:246–260. [PubMed: 19109973]

54. Mauk AG, Moore GR. Control of metalloprotein redox potentials: what does site-directed mutagenesis of hemoproteins tell us? J Biol Inorg Chem. 1997; 2:119–125.
55. Brown DI, Griendlin KK. Nox proteins in signal transduction. Free Radical Biol Med. 2009; 47:1239–1253. [PubMed: 19628035]
56. Murphy MP. How mitochondria produce reactive oxygen species. Biochem J. 2009; 417:1–13. [PubMed: 19061483]
57. Macosko EZ, Pokala N, Feinberg EH, Chalasani SH, Butcher RAJC, Bargmann CI. A hub-and-spoke circuit drives pheromone attraction and social behaviour in *C. elegans*. Nature. 2009; 458:1171–1175. [PubMed: 19349961]
58. Berman MC, Adnams CM, Ivanetich KM, Kench JE. Autoxidation of soluble trypsin-cleaved microsomal ferrocytochrome b5 and formation of superoxide radicals. Biochem J. 1976; 157:237–246. [PubMed: 183743]
59. Hargrove MS, Barry JK, Brucker EA, Berry MB, Phillips GN Jr, Olson JS, Arredondo-Peter R, Dean JM, Klucas RV, Sarath G. Characterization of recombinant soybean leghemoglobin a and apolar distal histidine mutants. J Mol Biol. 1997; 266:1032–1042. [PubMed: 9086279]
60. Smagghe BJ, Kundu S, Hoy JA, Halder P, Weiland TR, Savage A, Venugopal A, Goodman M, Premer S, Hargrove MS. Role of phenylalanine B10 in plant nonsymbiotic hemoglobins. Biochemistry. 2006; 45:9735–9745. [PubMed: 16893175]
61. Brantley RE Jr, Smerdon SJ, Wilkinson AJ, Singleton EW, Olson JS. The mechanism of autooxidation of myoglobin. J Biol Chem. 1993; 268:6995–7010. [PubMed: 8463233]
62. Mansouri A, Winterhalter KH. Nonequivalence of chains in hemoglobin oxidation. Biochemistry. 1973; 12:4946–4949. [PubMed: 4761975]
63. Fago A, Hundahl C, Dewilde S, Gilany K, Moens L, Weber RE. Allosteric regulation and temperature dependence of oxygen binding in human neuroglobin and cytoglobin. Molecular mechanisms and physiological significance. J Biol Chem. 2004; 279:44417–44426. [PubMed: 15299006]
64. Halder P, Trent JT III, Hargrove MS. Influence of the protein matrix on intramolecular histidine ligation in ferric and ferrous hexacoordinate hemogloins. Proteins. 2007; 66:172–182. [PubMed: 17044063]
65. Walker FA, Emrick D, Rivera JE, Hanquet BJ, Buttlaire DH. Effect of heme orientation on the reduction potential of cytochrome b5. J Am Chem Soc. 1988; 110:6234–6240.

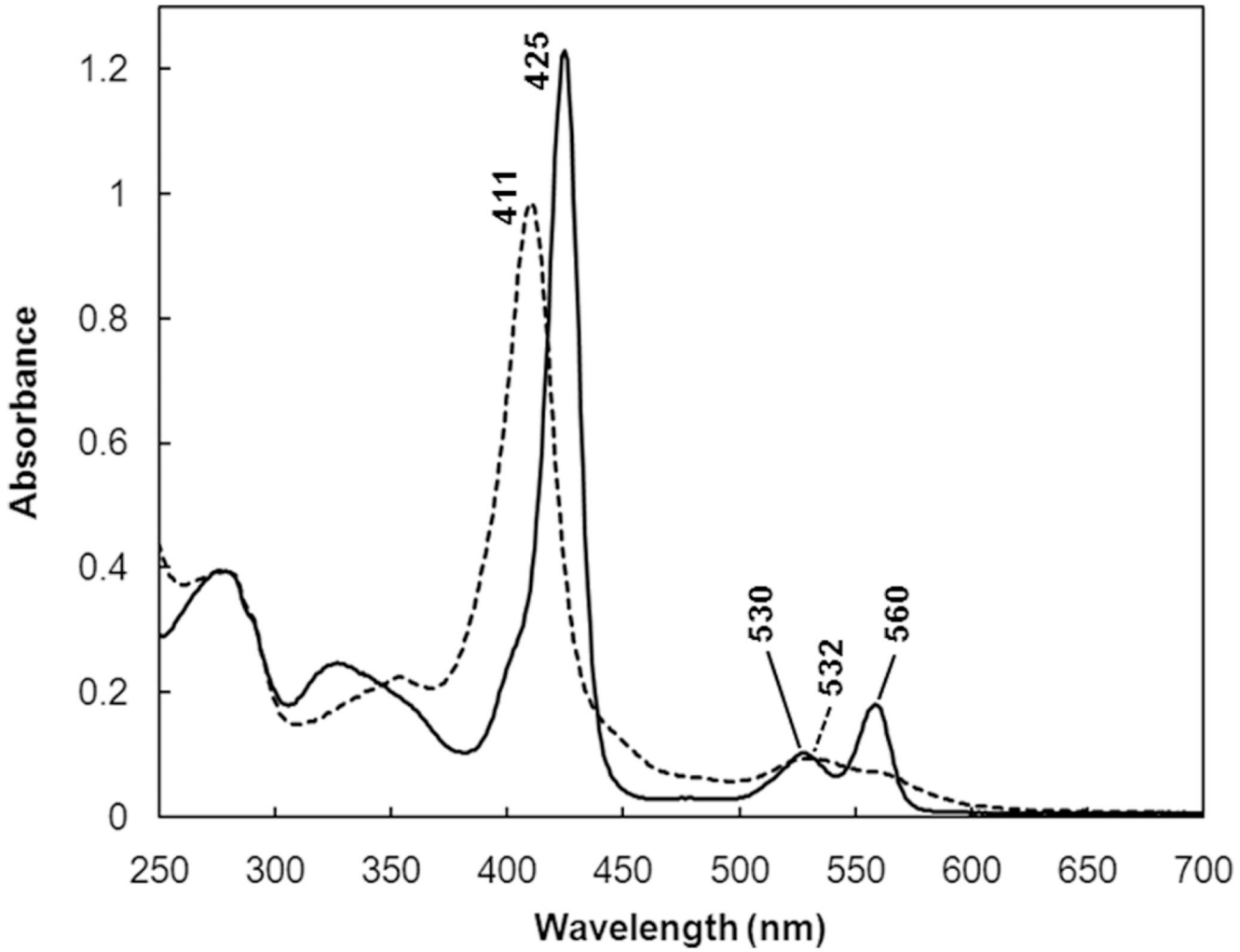

Figure 1.
UV-Vis absorption spectra of full-length ferrous GLB-6 (solid line) and ferric GLB-6 (dotted line). (Buffer = 20 mM HEPES, 150 mM NaCl, pH 7.5)

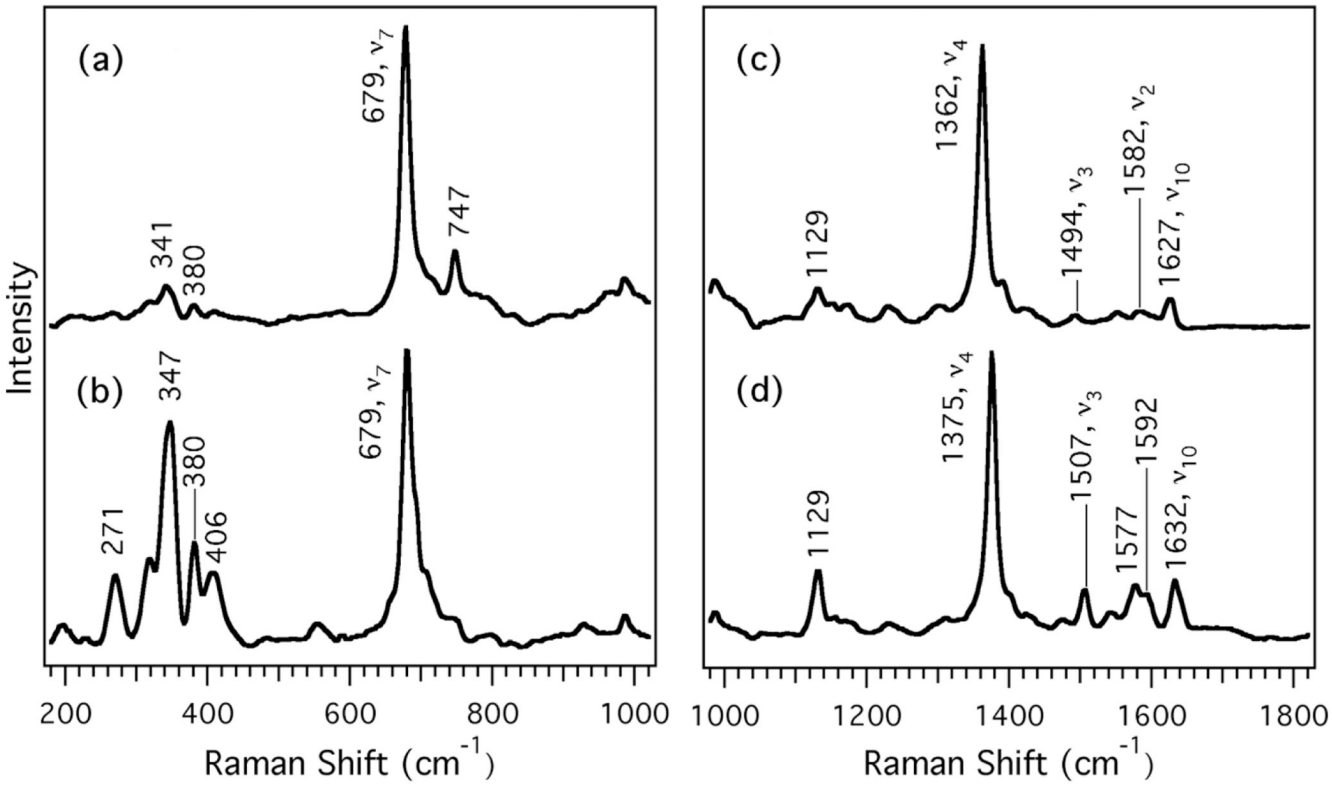

Figure 2.

Resonance Raman spectra of full-length ferrous GLB-6 (a, c) and ferric GLB-6 (b, d). The left panel (traces a and b) shows the lower frequency region and is normalized to ν_7. The right panel (traces c and d) shows the high frequency region and is normalized to ν_4. All spectra were acquired for 1 hour at room temperature with 413.1 nm excitation, room temperature, 2 mW.

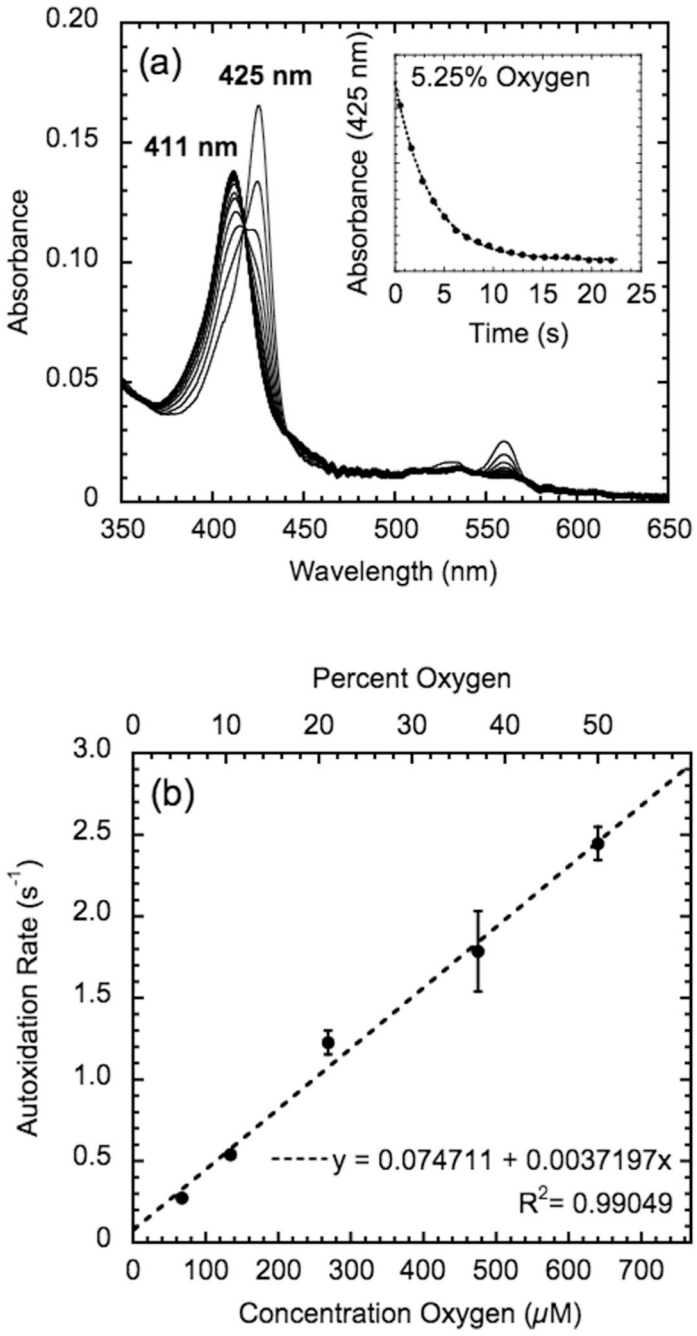

Figure 3.

Autoxidation rates of full-length GLB-6 measured by stopped-flow spectroscopy. (a) Spectral changes with time for the oxidation of ferrous GLB-6. Experiments were performed at 10 °C with different O_2 concentrations, 5.25, 10.5, 21.0, 37.1, and 50.0 % O_2. The spectral changes at 5.25 % O_2 are shown as representative data. The curve fitting of the change in A_{425} versus time using a single exponential model is shown in the inset. (b) The observed first-order autoxidation rate constant k_{obs} of full-length GLB-6 is plotted as a function of O_2 concentration. The fit to a linear function is shown as a dotted line.

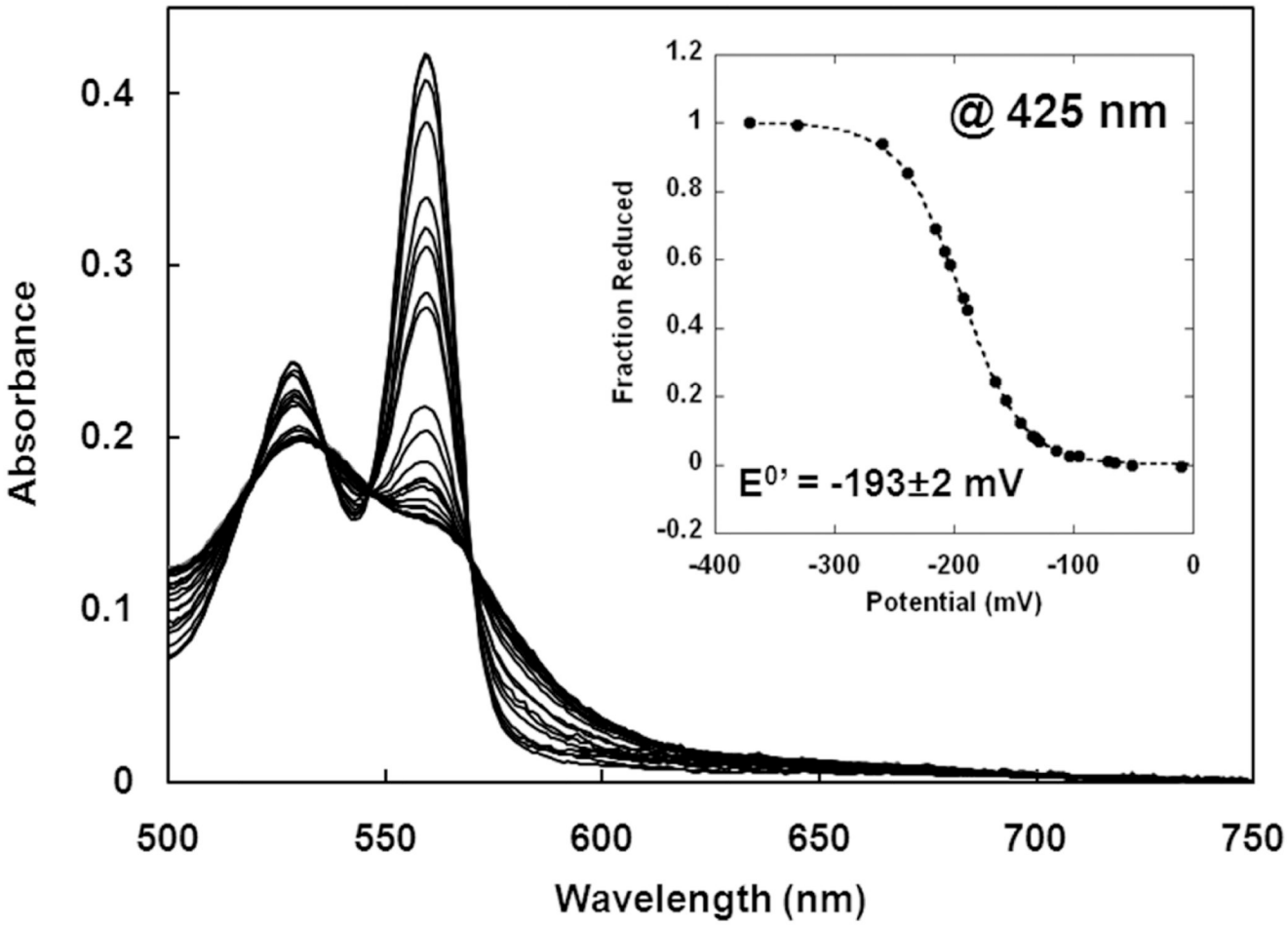

Figure 4.

Spectroelectrochemical potentiometric redox titrations of full-length GLB-6. The intensity of the α-band maxima, A_{560}, of ferrous GLB-6 minus A_{560} of ferric GLB-6 is normalized and plotted versus the ambient potential (inset). The data were analyzed for the best fit to Nernst equations with n = 1 (inset, dotted line). The measured redox potential versus SHE, $E^{0'}$, is −193 ± 2 mV, which is an average of three experiments. (Buffer: 100 mM potassium phosphate, 150 mM NaCl, pH 7.0, Temperature = 25 °C).

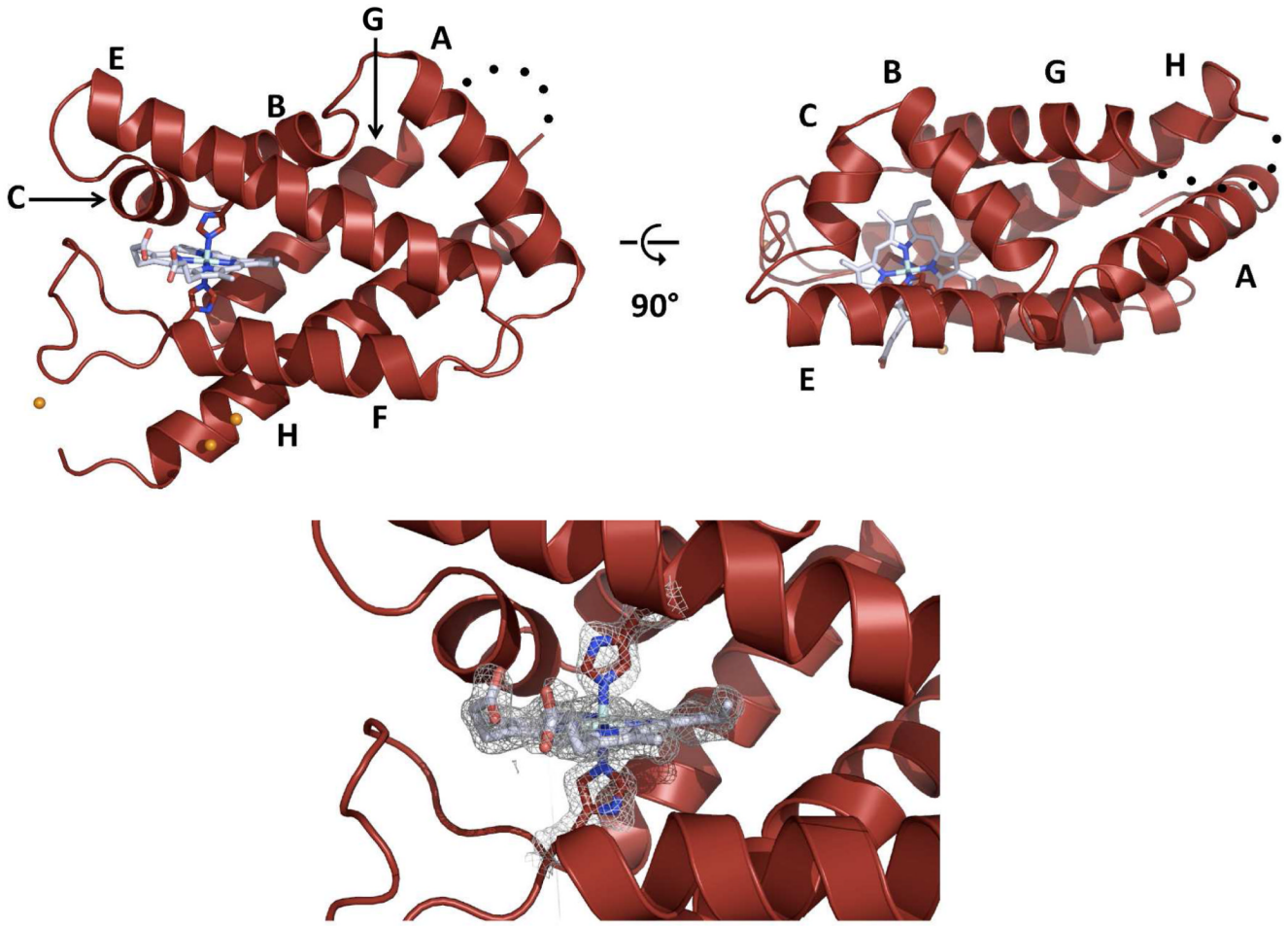

Figure 5.

Structure of the heme domain of GLB-6. Ribbon structure of the GLB-6 heme domain (molecule A) is shown with helices labeled according to the canonical globin fold. His254 and His289, distal (above) and proximal (below) heme ligands, respectively, and the heme moiety are shown as stick representation. Praseodymium atoms are represented as orange spheres. Note that residues 318–321 could not be traced and are shown as black dots. Lower panel shows $2F_o$-F_c composite simulated-annealing omit electron density map (1.0σ, gray mesh) calculated with heme moieties omitted.

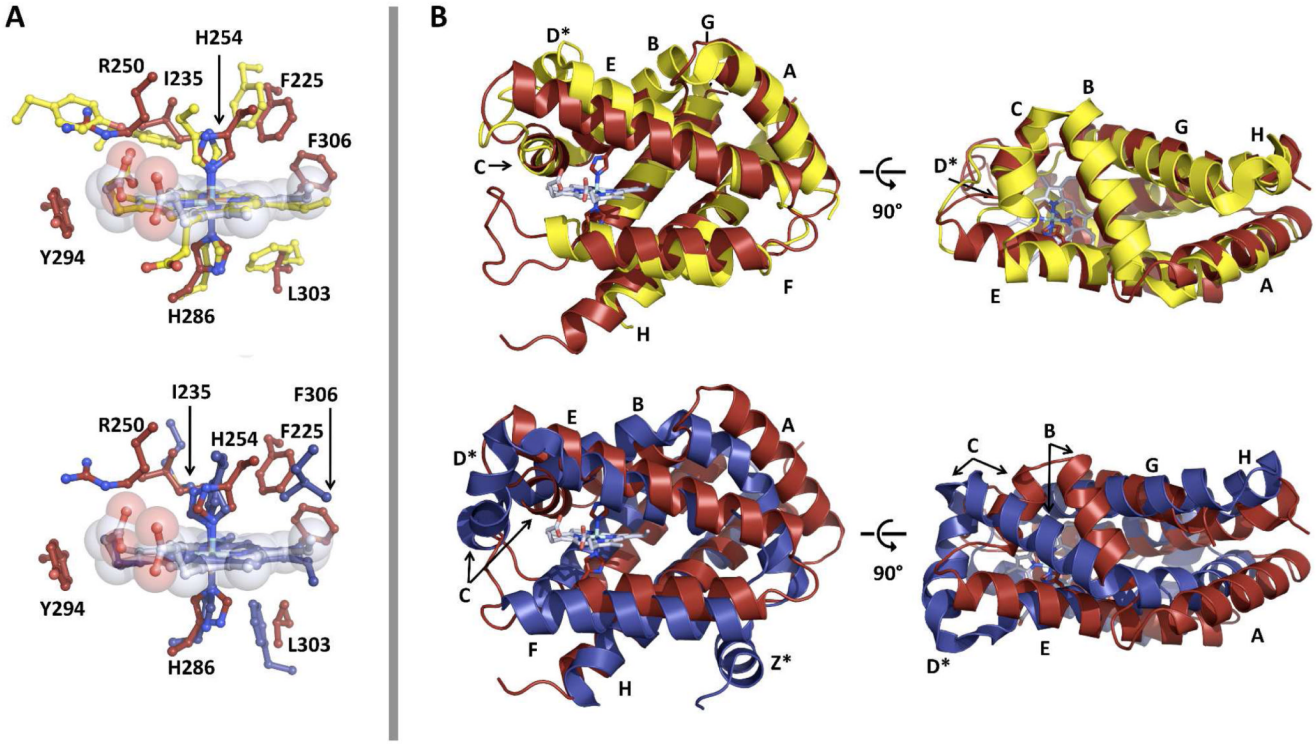

Figure 6.

Heme (a) and overall (b) alignments of GLB-6 (red) with murine neuroglobin (yellow, PDB: 1Q1F) (top) and *Geobacter sulfurreducens* globin-coupled sensor (blue, PDB: 2W31) (bottom). Only residue assignments for GLB-6 are provided for clarity. Helices are labeled according to Figure 5. D-and Z-helices are marked with an asterisk to indicate that they do not exist in the GLB-6 structure.

Table 1

Autoxidation rates of selected globins.

Protein	Autoxidation Rate (hr^{-1})	Reference
GLB-6 (1–389)	4,428	this work
Cyt b_5[a]	20	(58)
mNgb[b]	19	(5)
hNgb[c]	5.4	(5)
Lb[d]	0.2	(59)
rice Hb[e]	0.08	(60)
Sw Mb[f]	0.055	(61)
hHb (α chain)[g]	0.032	(62)
hHb (β chain)[g]	0.0037	(62)
Cgb[h]	stable[i]	(6,63)

[a] trypsin-cleaved calf liver cytochrome b_5,

[b] mouse neuroglobin,

[c] human neuroglobin,

[d] soybean leghemoglobin,

[e] rice non-symbiotic hemoglobin,

[f] sperm whale myoglobin,

[g] human hemoglobin,

[h] human cytoglobin,

[i] negligible autoxidation observed (>1000 s)

Table 2

Redox potentials of various heme proteins.

Protein	Axial Ligation	$E^{0'}$ (mV)	Reference
GLB-6 (1–389)	His/His	−193 ± 2 mV	this work
Truncated Hb[a]	His/His	−195	(64)
Rice Hb[b]	His/His	−143	(64)
Ngb[c]	His/His	−115	(64)
Cgb[d]	His/His	−28	(64)
Cyt b_5[e]	His/His	−2	(64)
Mb H64V/V68H[f]	His/His	−128	(52)
Mb wt	(H_2O)/His	+54	(52)
CDH M65H[g]	His/His	−53	(49)
CDH wt	His/Met	+164	(49)
Cyt c_{551} M61H[h]	His/His	+55	(50)
Cyt c_{551} wt	His/Met	+260	(50)
Cyt c M80H[i]	His/His	+41	(51)
Cyt c wt	His/Met	+260	(51)

[a] truncated hemoglobin from the cyanobacterium *Synechocystis*,

[b] rice non-symbiotic hemoglobin,

[c] human neuroglobin,

[d] human cytoglobin,

[e] bovine erythrocyte cytochrome b5,

[f] human/pig myoglobin,

[g] cellobiose dehydrogenase from white rot fungus *Phanerochaete chrysosporium*,

[h] cytochrome c551 from bacterium *Pseudomonas stutzeri*,

[i] cytochrome c from horse heart.

Table 3

Data collection, phasing, and refinement statistics.

Data Collection and Refinement		Praseodymium	GLB-6 (187–355)
Data Collection	Wavelength	1.1158	0.9765
	Resolution (Å)	50.0–1.69 (1.72–1.69)	33.7–1.40 (1.42–1.40)
	Space Group	$P2_1$	$P2_1$
	Cell Dimensions		
	a, *b*, *c* (Å)	37.55, 76.77, 62.68	37.58, 76.34, 62.69
	β(°)	91.6	91.7
	Redundancy	3.6 (3.3)	4.2 (4.0)
	Completeness[a] (%)	98.6 (82.8)	97.0 (95.1)
	R_{sym} (%)	5.4 (21.3)	5.3 (29.4)
	I/σ[a]	19.9 (5.9)	21.5 (3.6)
Refinement	No. of Reflections		127215
	R_{work}/R_{free}[b] (%)		16.1/20.1
	No. Atoms		
	Protein		2560
	Heme		86
	Praseodymium		4
	Solvent Molecules		139
	B-factors		
	Protein		25.7
	Water		51.6
	Overall		31.8
	Rms Deviation		
	Bond Lengths (Å)		0.005
	Bond Angles (°)		0.863

[a] The values in parentheses relate to highest-resolution shells.

[b] R_{free} is calculated for a randomly chosen 5% of reflections.